Article:
Ismail, M.S. orcid.org/0000-0002-9539-8925, Mohamed, A.M., Poggio, D. et al. (2 more authors) (2022) Modelling mass transport within the membrane of direct contact membrane distillation modules used for desalination and wastewater treatment : scrutinising assumptions. Journal of Water Process Engineering, 45. 102460. ISSN 2214-7144

https://doi.org/10.1016/j.jwpe.2021.102460

Modelling mass transport within the membrane of direct contact membrane distillation modules used for desalination and wastewater treatment: scrutinising assumptions

M.S. Ismail [a, b *], A.M. Mohamed [c], D. Poggio [a], M. Walker [d], M. Pourkashanian [a, b]

[a] Energy Institute, University of Sheffield, Sheffield S3 7RD, United Kingdom
[b] Translational Energy Research Centre (TERC), University of Sheffield, Sheffield S3 7RD, United Kingdom
[c] Faculty of Engineering, Port Said University, Port Said, Port Foad 42526, Egypt
[d] Department of Engineering, University of Hull, Hull HU6 7RX, United Kingdom

[*] Corresponding author: Tel: +44 114 21 57242
Email addresses: m.s.ismail@sheffield.ac.uk, msaeedaaal@gmail.com (M.S. Ismail)

Abstract

A two-dimensional numerical model for a direct contact membrane distillation (DCMD) module, mostly used for desalination and wastewater treatment, has been created. This model has been used to explore the sensitivity of the simulated transmembrane flux of water vapour of the modelled distillation module to some of the commonly-used assumptions and simplifications related to the mass transport in the membrane, namely: equimolar diffusion; Knudsen diffusion-free mass transport; and binary gas mixture. The model has been also used to assess the impact of a slight total pressure difference across the membrane. The sensitivity of the transmembrane flux to the above assumptions has been then evaluated with relatively low and high inlet feed temperatures. The outcomes of the model have been presented, discussed and finally summarised.

Keywords: Direct contact membrane distillation; Numerical model; Mass transport; Diffusion; Transmembrane flux

1. Introduction

Membrane distillation (MD) is a distillation method in which the driving force is the difference in vapour pressure across the sides of the membrane which exponentially changes with temperature [1]. MD has been demonstrated in many applications, in particular desalination and wastewater treatment [2,3,4]. MD, compared to reverse osmosis which is the most dominant membrane based technology for desalination and wastewater treatment, features: (i) less sensitivity to high solute concentrations, (ii) almost perfect rejection of non-volatile solutes (e.g. salt, macromolecules and colloids) and (iii) possible use of renewable energy and/or low grade heat [5-6]. The membranes used in MD modules are typically microporous and hydrophobic [7]. There are four major configurations of MD system that differ on how vapour permeated across the membrane is processed in the cold side: (i) direct contact membrane distillation (DCMD) where both the hot feed stream and the cold permeate stream are in direct contact with the membrane [7], (ii) air gap membrane distillation (AGMD) where an air gap is placed between the membrane and a condensation surface [8], (iii) vacuum membrane distillation (VDM) where the vapour phase is vacuumed from the liquid through the membrane and is, if needed, condensed externally [9] and (iv) sweeping gas membrane distillation (SGMD) where an inert gas is used to sweep the produced vapour which is, if needed, condensed externally [10]. The configuration investigated in the paper is the DCMD which is, compared to other configurations, simpler and/or requires less auxiliary components (e.g. vacuum pumps, gas compressor or external condensers). As mentioned earlier, in addition to desalination applications, the use of DCMD for wastewater treatment has been reasonably demonstrated [11]. Namely, DCMD was used to treat olive mill wastewater, which is charactersied by low pH and high biological oxygen demand (BOD) and chemical oxygen demand (COD) levels [12]. A DCMD module (in which the permeate stream was injected with 0.01 mol/litre sulphuric acid) was shown to remove ammonia, which is a common pollutant in

industrial and municipal wastewater, with high efficiency (99.5%) [13]. Likewise, DCMD was proven to be successful treating low level radioactive wastewater [14] and textile wastewater containing synthetic dyes [15].

Modelling the mass transport across the membrane has received most of the interest by the MD modellers [16] as it is associated with the most important key performance indicator: the transmembrane flux. In the DCMD modules, designed for desalination and wastewater treatment, the saturation pressure of water vapour at both sides of the membrane scales exponentially with temperature and as a result a gradient in this saturation pressure is created across the membrane, driving water vapour from the relatively hot side of the membrane to the relatively cold side of the membrane. The mass transport within the membranes of the modelled DCMD modules is normally assumed to be governed by one or a combination of the following physics: molecular diffusion, Knudsen diffusion and viscous flow. The rationales behind selecting some or all these physics are described below.

As the average pore size of typical membranes (0.1 – 1 μm) is of the same order as the mean free path [17] (i.e. the distance travelled by a molecule between successive collisions [16]) both molecular and Knudsen diffusion co-exist and govern the transport of water vapour in the membrane. To illustrate, the mean free path of water vapour at 1 bar and 25°C is about 0.13 μm [17,18] which is of the same order as the average pore size of the membrane. In other cases, the feed and the permeate streams are (or are assumed to be) deaerated and therefore the molecular diffusion is neglected and the Knudsen diffusion and viscous flow are considered for the transport of water vapour in the membrane. Deaerating the feed and the permeate streams significantly increases the mean free path of the diffusing molecules, causing Knudsen diffusion to be the most dominant mode of diffusion. Further, deaerating the streams results in a total pressure difference across the membrane that induces viscous flow. As will be shown in the next two paragraphs, the literature has shown a great deal of discrepancy in terms of

selection of the physics simulating the mass transport of water vapour across the membrane. Single or multiple different physics are, either depending on some assumptions or even arbitrarily, used to model the mass transport of water vapour within the membrane.

Park et al. [2] developed a two-dimensional numerical model for a DCMD module and computed the transmembrane flux of water vapour using an expression that was originally derived by Phattaranawick et al. [19] and represents the transition regime where both molecular and Knudsen diffusions are important to be considered. Liu and Wang [14] used the same above-mentioned expression to model the transport of water vapour within a membrane of a distillation module used to treat low-level radioactive wastewater. Considering deaerated streams, Chen et al. [20] modelled the transport of water vapour within the membrane using a combination of Knudsen diffusion and viscous (or Poiseuille) flow. This approach was also adopted by other researchers [21,22,23].

Alklaibi and Lior [24] used an expression for molecular diffusion to model the transmembrane flux. Notably, Hayer et al. [25] considered a combination of molecular and Knudsen diffusion as well as a convective flux (using Darcy's law) to model the flux of water vapour in the membrane. However, it was not clear whether they used total pressure or partial pressure of water vapour to compute the velocity of water vapour. Perfilov et al. [26] started their analysis for the flow of water vapour with dusty gas model (DGM) [27] (i.e. Eq. (28) in [26]); however they, after stating some assumptions, used a similar expression (i.e. Eq. (33) in [26]) to that of Hayer et al. [25] to compute the transmembrane flux of water vapour. On the other hand, some investigators used experimentally determined coefficients that lump all the diffusive and convective flow effects when modelling the transmembrane flux of water vapour; this coefficient may be called intrinsic mass transfer coefficient [28], membrane distillation coefficient [5], membrane transfer coefficient [15] or simply permeability [16].

The main motive of this work is to investigate the sensitivity of the outputs of the modelled DCMD module (in the form of the transmembrane flux) to the main assumptions that are sometimes made when modelling the transport of water vapour in the membrane. Namely, the mass transport within the membrane is sometimes assumed to be equimolar counter-diffusion that is the diffusion fluxes of water vapour and air are equal and as such there is no net diffusion flux. Further, as shown in the literature review made above, Knudsen diffusion is sometimes ignored, meaning that the collisions of the diffusing molecules with the walls of the pores media are neglected; we investigate the impact of this neglect on the outcomes of the modelled DCMD module. Also, the gas mixture is mostly assumed to be binary consisting of only water vapour and air rather than ternary (water vapour, nitrogen and oxygen gases), allowing for a simpler equation of Fick's law to be used to estimate the transmembrane flux of water vapour; the sensitivity of the latter parameter to this assumption is explored through using a set of equations describing the diffusion of ternary gas mixture (Maxwell-Stefan equations). Finally, some light is shed on the possibility that the membrane may experience a slight total pressure difference that may boost the transmembrane flux of water vapour. This study provides a scope on the validity of all the above assumptions and when one should (i) use some or all of these assumptions to simplify the solution of the model and/or save the computation time or (ii) use more rigorous physics to avoid obtaining inaccurate or unrealistic predictions. This knowledge evidently assists in proposing well-informed designs for DCMD modules.

2. Model formulation

We considered a geometry for a DCMD module that has been recently used in a previous work [29]. Most of the details describing the governing equations and the boundary conditions are presented here for completeness and to maintain the flow of the ideas. However, non-equimolar (rather than equimolar) diffusion was considered to simulate the transport of the gas mixture in the membrane. As mentioned in the introduction, the sensitivity of the outcomes of the model

(in terms of the transmembrane flux of water vapour) to the equimolar diffusion assumption is explored (Section 3.1).

Below is the description of the equations used for the simulations. The flow in the feed and the permeate channels is considered to be steady, laminar and incompressible and therefore the conservation of mass and momentum equations are of the following forms:

$$\rho \nabla . (\boldsymbol{u}) = 0 \tag{1}$$

$$\rho (\boldsymbol{u}. \nabla) \boldsymbol{u} = \nabla . (-p\boldsymbol{I} + \mu(\nabla \boldsymbol{u} + (\nabla \boldsymbol{u})^T)) \tag{2}$$

where ρ and μ are the density and the dynamic viscosity of the flowing fluid and $\boldsymbol{u}$ is the velocity vector, p is the pressure and $\boldsymbol{I}$ is the identity tensor. The transfer of heat is governed by the conservation of energy equation:

$$\rho . C_p . \boldsymbol{u} . \nabla T + \nabla . (-k \nabla T) + S_T = 0 \tag{3}$$

Where T is the temperature, C_p is the specific heat capacity at a constant pressure (J kg^{-1} K^{-1}), and k is the thermal conductivity. ρ, μ, C_p and k of liquid water are, assuming negligible effects of the solute (i.e. salt), given using the temperature-dependent polynomials stated in Appendix A. The effective thermal conductivity of the membrane (k_{eff}) is obtained as follows:

$$k_{eff} = \varepsilon k_g + (1 - \varepsilon) k_s \tag{4}$$

where ε is the porosity, k_s is the thermal conductivity of the material of the membrane and k_g is the thermal conductivity of the gas mixture which is, for simplicity, assumed to be that of the most dominant component (i.e. air) for the given operating temperatures (20-80 °C) [30]:

$$k_g = -2.276 \times 10^{-3} + 1.155 \times 10^{-4} T - 7.903 \times 10^{-8} T^2 + 4.117 \times 10^{-11} T^3 - 7.439 \times 10^{-15} T^4 \tag{5}$$

S_T is the heat source term and is zero in the channels and equals to the special change rate of the vaporisation heat in the membrane:

$$S_T = \nabla.(h_{fg}J) \tag{6}$$

where h_{fg} is the latent heat of vaporisation (kJ kg^{-1}) and J is the transmembrane flux of water vapour (kg m^{-2} s^{-1}). As mentioned in [29], unlike previous models, the change of h_{fg} with temperature and space was accounted for in this model; it was not simply assumed to be constant or divided by the membrane thickness. h_{fg} changes with temperature following the equation that was fitted using some tabulated data for saturated water vapour [31]: $h_{fg} = 2.4324T - 3167.2$. The convective term, the first term in Eq. (3), was assumed to be negligible within the pores of the membrane as the total pressure difference across the membrane is zero. The transmembrane flux of water vapour is given by:

$$\nabla.(N) = 0 \tag{7}$$

$$N = -D_{eff}\nabla C_w \tag{8}$$

$$J = N.M_w \tag{9}$$

where J and N are the mass and molar flux of water vapour respectively, M_w is the molecular weight of water and D_{eff} is the effective diffusivity of water vapour which was, considering the molecule-wall collisions, derived and given by [19] as:

$$D_{eff} = \frac{\varepsilon}{\tau}\left[\frac{1}{D_{Kn}} + \frac{1-(1-\beta)y_w}{D_{w-a}}\right]^{-1} \tag{10}$$

where ε and τ are the porosity and tortuosity of the membrane, y_w is the mole fraction of water vapour and β is the ratio of the diffusion rate of air to the diffusion rate of water (Graham's law) and is given by [19]:

$$\beta = \sqrt{\frac{M_w}{M_a}} \tag{11}$$

where M_a is the molecular weight of air. D_{w-a} is the molecular diffusion coefficient of water vapour into air which varies with temperature as follows [32]:

$$D_{w-a} = 1.895 \times 10^{-5} \frac{T^{2.072}}{101325} \quad (12)$$

D_{Kn} is the Knudsen diffusion coefficient [19]:

$$D_{Kn} = \frac{4d_p}{3} \sqrt{\frac{RT}{2\pi M_w}} \quad (13)$$

where d_p is the pore diameter of the membrane and R is the universal gas constant (8.3145 J mol^{-1} K^{-1}). C_w is the water vapour concentration and is given by:

$$C_w = a_w y_w \frac{p_s}{RT} \quad (14)$$

where a_w and y_w are the activity coefficient and mole fraction of liquid water; they are both (assuming 100% purity for water) equal to unity at the interface between the membrane and the permeate channel. The activity coefficient for non-ideal aqueous electrolyte and nonelectrolyte solutions (including saline and wastewater water) could be approximated using the following equation [33]:

$$a_w = (1 - y_s) exp(\alpha y_s^2 + \beta y_s^3) \quad (15)$$

where y_s is the molar fraction of the solute (e.g. salt or urea) and α and β are experimentally determined parameters. Miyawaki et al. [33] listed the α and β parameters for a wide range of non-ideal aqueous electrolyte and nonelectrolyte solutions. However, the following expression for activity coefficient is typically used for saline water and was used in this work [16]:

$$a_w = 1 - 0.5 y_{NaCl} - 10 y_{NaCl}^2 \quad (16)$$

where y_{NaCl} is the mole fraction of the solute (NaCl); it was estimated to be 0.011 for 3.5 wt. % NaCl solution. Note that the variation in the computed transmembrane flux of water vapour when using Eq. (15) or Eq. (16) is less than 1%. It should be also noted we considered saline water for the feed channel of the module as the reported experimental data (with which we could validate our model) associated with the DCMD modules used for desalination demonstrations are significantly more than those used for wastewater treatment. However, the

findings in this work should be applicable to both applications (i.e. desalination and wastewater treatment) as the activity coefficient is very slightly sensitive to the type of the solute in the low concentration aqueous solutions [33], resulting in marginal variations in the outcomes of the model. The saturation pressure of water vapour, p_s, is estimated using Antoine equation [16]:

$$p_s = exp\left(23.1964 - \frac{3816.44}{T - 46.13}\right) \tag{17}$$

Boundary conditions and solution procedure

The boundary conditions used to solve the conservation equations are shown in Fig. 1a. Inlet temperatures (T_{hi} and T_{ci}) and velocities ($\boldsymbol{u}_{hi}$ and $\boldsymbol{u}_{ci}$) are prescribed at the inlets of the channels and zero pressures are prescribed at the outlets of the channels. No slip boundary conditions are prescribed at the walls of the channels. Molar concentrations, calculated by Eq. (14), are prescribed at the left (C_{wl}) and the right (C_{wr}) sides of the membrane. No heat flux ($-\boldsymbol{n}.q = 0$) and no molar flux ($-\boldsymbol{n}.N = 0$) are appropriately implemented as shown in Fig. 1a.

The modelled geometry was meshed as presented in Fig. 1b. The mesh is made significantly finer at the interfaces and the boundaries in order to capture the expected high rates of change in these regions. The number of elements is 9000 which is found to give a mesh-independent solution. Eq. (1), Eq. (2), Eq. (3) and Eq. (7) were discretised and solved using COMSOL Multiphysics 5.2a® solver.

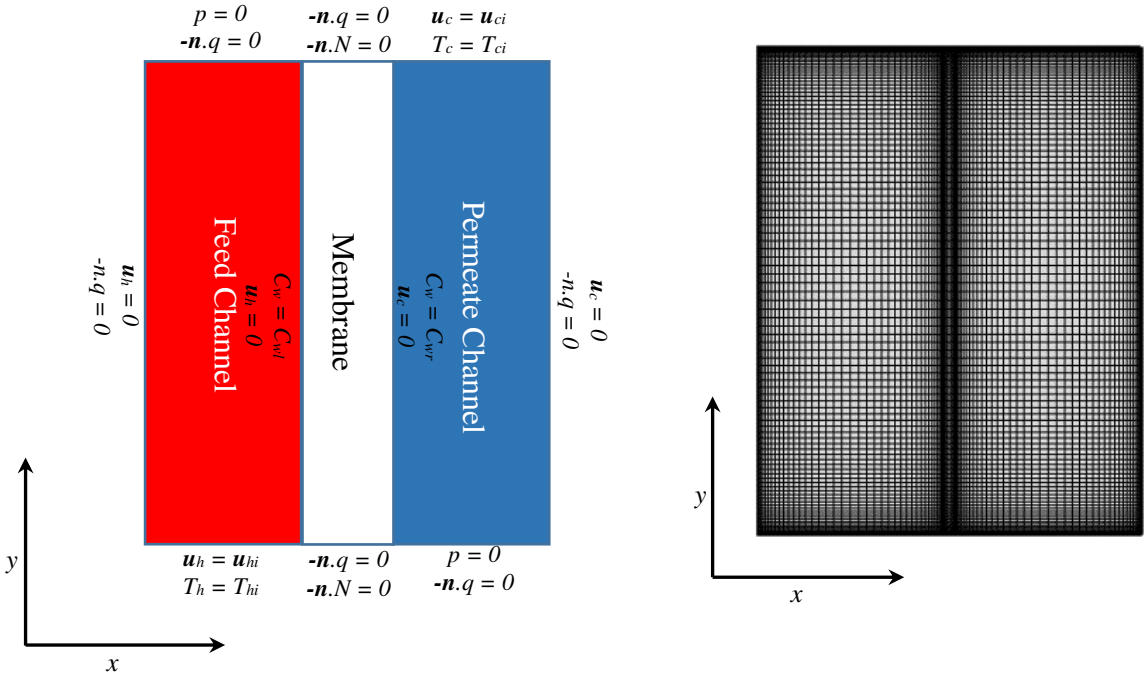

(a) (b)

Fig. 1 (a) The boundary conditions used to solve the model (the schematic is not to scale). *N* is the molar flux and equal to $-D_{eff}\nabla C_w$ and *q* is heat flux and equal to $-k\nabla T$ and (b) the meshed computational domain. Note that the dimensions in x-direction (i.e. the height of each channel, 0.002 m, and the membrane thickness, 130 μm) are, compared to the length of the module in the y-direction (i.e. 0.21 m), scaled up 40 times in order to present a clearer view of the mesh.

3. Results and discussion

The accuracy of the developed model has been already assessed in [29]. As mentioned in Section 2, non-equimolar diffusion (rather than equimolar diffusion that was adopted in [29]) was considered for the transport of gas mixture within the membrane. Therefore, it is, considering this change, important to reproduce the validation plots in the present work. Multiple sets of experimental data taken from [20] and [34] were used for validation. Fig. 2 shows good agreement between the measured [20] and the computed transmembrane fluxes as they change with the inlet velocities and the inlet feed temperatures; the key trends are captured by the model and the variance for any two sets of modelling and experimental is less than 10% which is better than that reported in [29]: 15%. Likewise, slightly better agreement is, compared to that demonstrated in [29], observed between the computed transmembrane flux and the measured transmembrane flux reported in [34] particularly for the case where the inlet feed

temperature is 40 °C (Fig. 3a). Further, Fig. 3b shows very good agreement between the experimental [34] and the modelling data of the outlet temperatures of the feed and the permeate channels as they change with the inlet velocities. As mentioned in [29], the geometry of the DCMD module reported in [20] was considered in the present work and this is owing to the availability of all the physical parameters required for building and running the model; note that the developed model was slightly adapted for the DCMD module reported in [34] in order to account for the changes in the values of some parameters (see the caption of Fig. 3).

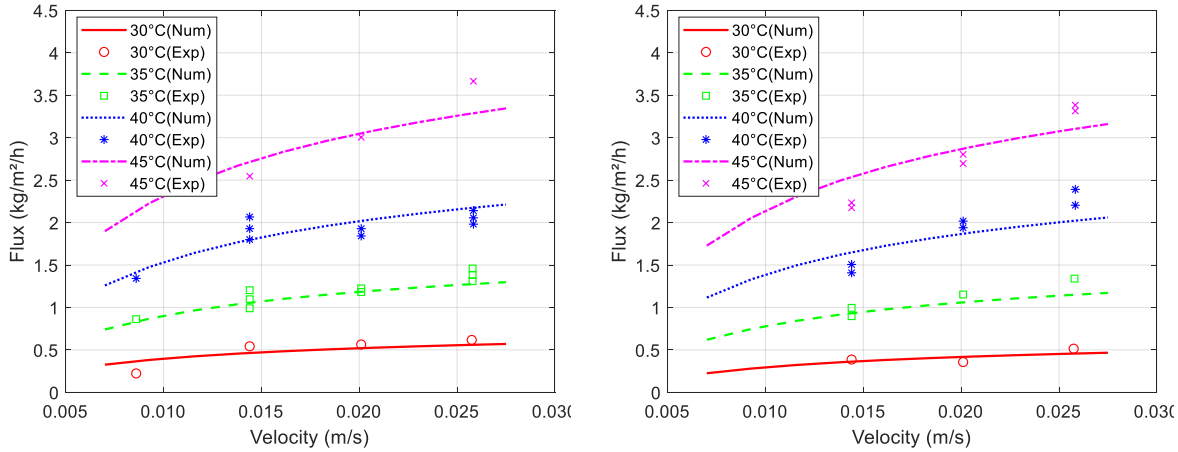

(a) (b)

Fig. 2 The transmembrane flux as a function of inlet velocity and feed temperature for: (a) fresh water and (b) saline solution (3.5 wt. % NaCl) as a feed stream. Note that the inlet permeate temperature was kept constant at 25 °C and the flow configuration was co-flow [20]. Note that the modelling data shown in these figures are slightly different to those reported in [29] and this is due to considering non-equimolar diffusion for the transport of gas mixture within the membrane in the present work.

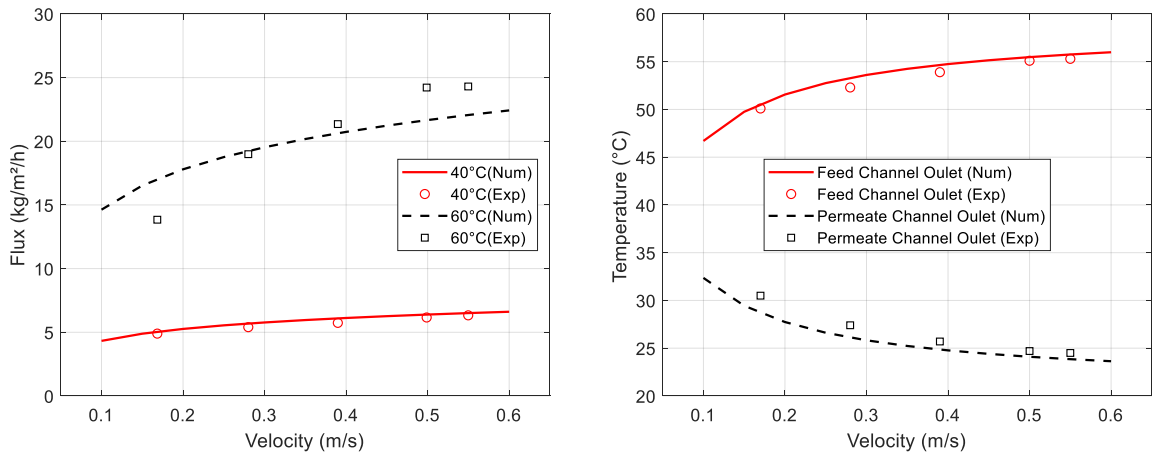

(a) (b)

Fig. 3 (a) The transmembrane flux as a function of inlet velocity for two inlet feed temperatures (40 and 60°C) and (b) the outlet temperatures of the feed and permeate channels as they change with inlet velocities. The width and the height of each channel in the module reported in [34] are 1 mm and 0.4 m, respectively. The salinity (w_s), the average pore diameter of the membrane (d_p), the membrane thickness (t_m), the porosity of the membrane (ε), the tortuosity of the membrane (τ) and thermal conductivity of the membrane material (k_s) used for the respective model are: 1%, 0.28

μm, 100 μm, 0.72, 1.4 and 0.178 W m^{-1} K^{-1}, respectively. Note that the modelling data shown in these figures are slightly different to those reported in [29] and this is due to considering non-equimolar diffusion for the transport of gas mixture within the membrane in the present work.

Table 1 lists the physical parameters used for the base case of the model. It should be noted that, following the normal practice, the flow configuration was counter-current. The water vapour concentration within the membrane and the velocity and the temperature contours were generated in our previous work [29] and have been re-produced in this work (Appendix B) for completeness. There are slight differences between two sets of graphs used in this article and the previous article and this is due to the fact that non-equimolar diffusion (rather than equimolar diffusion) was used in the present work. However, the general trends are similar in both sets. Namely: (i) the flow becomes hydrodynamically fully developed after a short distance from the inlets (Fig. A1(a)), (ii) the flow is thermally developing (Fig. A1(b)) and (iii) the flux of water vapour within the membrane is a maximum just before the outlet of the permeate channel and just after the inlet of the feed channel (Fig. A1(c)). The latter observation is corroborated by the profile of water vapour flux at the interface between membrane and the feed channel (Fig. A1(d)). Interestingly, Fig. A1(d) also shows that the flux of water vapour starts to slightly increase as the region, where feed stream exits its channel and permeate stream enters its channel, is approached (> 0.2 m). This is due to the fact that the temperature of the permeate channel is a minimum at the inlet (20°C) and this in turn creates a difference in saturation pressure of water vapour that is sufficiently high to induce a relatively high water vapour flux compared to the other regions close to the inlet of the permeate channel/the exit of the feed channel.

Table 1 The parameters used for the modelled DCMD.

Parameter	Value
Channel height	0.002 m [20]
Module length	0.21 m [20]
Membrane porosity (ε)	0.72 [20]
Membrane thickness	130 μm [20]

Average pore dimeter (d_p)	0.1 μm [20]
Thermal conductivity of membrane material (k_s)	0.178 W m^{-1} K^{-1} [20]
Salinity	3.5 wt. % [20]
Inlet velocity of feed stream ($\boldsymbol{u}_{hi}$)	0.2 m s^{-1}
Inlet velocity of permeate stream ($\boldsymbol{u}_{ci}$)	0.2 m s^{-1}
Inlet temperature of feed stream (T_{hi})	60 °C
Inlet temperature of permeate stream (T_{ci})	20 °C

3.1 Non-equimolar diffusion versus equimolar diffusion

Fig. 4 shows the change of water vapour flux $\bar{J}$ (averaged over the length of the membrane) with the average pore diameter of the membrane (d_p) for two cases: a case in which the diffusion is non-equimolar (the base case) and a case in which the diffusion is assumed to be equimolar. For the latter case, Eq. (10) simplifies to:

$$D_{eff} = \frac{\varepsilon}{\tau}\left[\frac{1}{D_{Kn}} + \frac{1}{D_{w-a}}\right]^{-1} \tag{18}$$

The figure also presents the relative error that is incurred as a result of the equimolar diffusion assumption; it is mathematically defined as $100 \times \left(\bar{J}_{non-eq} - \bar{J}_{eq}\right)/\bar{J}_{non-eq}$, where the subscripts "non-eq" and "eq" stand for non-equimolar and equimolar respectively. Similar expressions to calculate and plot the relative errors/gains were used in Sections 3.2, 3.3, 3.4 and 3.5. Note that the fluxes (equimolar and non-equimolar) as well as the relative error share the y-axis. The results show that the equimolar diffusion assumption may be tolerated for the membrane with relatively low pore size (< 0.1 μm) as the mass transport is dominated by Knudsen diffusion (where molecule-wall collisions prevail over molecule-molecule collisions). As the pore size increases beyond 0.1 μm, the molecular diffusion starts to play a more profound role in transporting water vapour across the membrane; therefore, in such cases, the error in estimating $\bar{J}$ as a result of equimolar diffusion assumption cannot be overlooked. The pore size of most of the membranes are typically between 0.1 and 1 μm (see for example Table 2 in [35]). Therefore, $\bar{J}$, with equimolar diffusion assumption, for membranes with 0.1

and 1 μm average pore diameters are underestimated by around 8 and 17 % respectively. It is noteworthy that the flux of water vapour considering non-equimolar diffusion is larger than flux of water vapour assuming equimolar diffusion especially in molecular diffusion dominated region (d_p > 1 μm); this is due to the fact the molecular diffusion rate of water vapour is, according to Graham's law (i.e. Eq. (11)), is higher than that of air by a around 1.3. One final remark in this section is that the increase rate of the relative error becomes less and that the relative error approaches a constant value as d_p increases; this is due to diminishing effects of Knudsen diffusion. In other words, the relative error is constant if Knudsen diffusion is neglected.

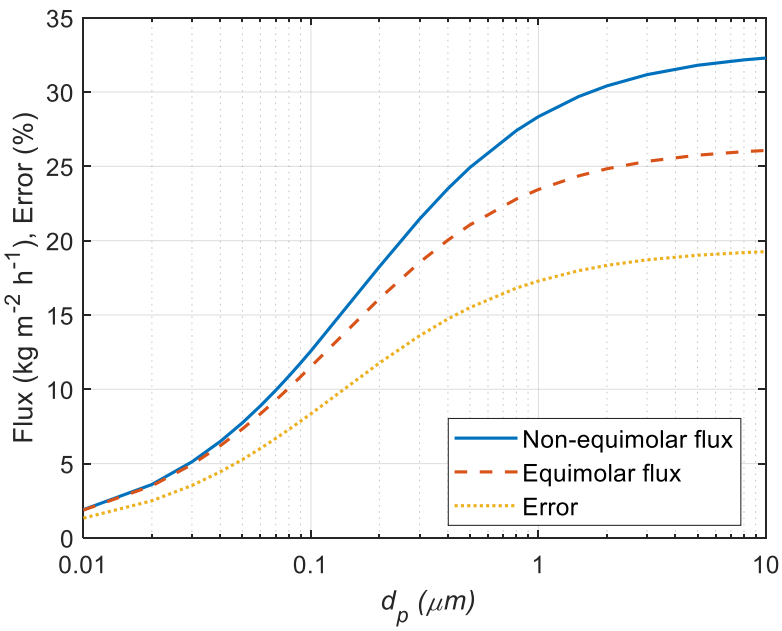

Fig. 4 The transmembrane flux of water vapour ($\bar{J}$) as it changes with the average pore diameter of the membrane (d_p) for the cases where the diffusion is non-equimolar (solid line) and equimolar (dashed line).

3.2 Knudsen diffusion effects

If Knudsen diffusion is ignored, Eq. (10) simplifies to:

$$D_{eff} = \frac{\varepsilon}{\tau}\left(\frac{D_{w-a}}{1-(1-\beta)y_w}\right) \tag{19}$$

Fig. 5a shows how $\bar{J}$ changes with d_p, with/without considering Knudsen diffusion. Clearly, for relatively small values of d_p, $\bar{J}$ is massively overestimated if Knudsen diffusion is neglected. Knudsen number (Kn) is normally used to identify diffusion regimes: molecular, slip, transition or Knudsen [36]. The transition regime is, in general, where both molecular and Knudsen diffusions play an important role in transporting the gaseous species. Kn is mathematically expressed as [18]:

$$Kn = \frac{\lambda}{d_p} \tag{20}$$

where λ is the mean free path of the diffusing molecules. λ for water vapour is about 0.145 µm at 60 °C and 1 atm (calculated based on the relevant data provided in Chapter 17 in [18]). For typical operating temperatures of DCMD (20-80 °C), λ for water vapour slightly changes with temperature (~ 10 %) and it is therefore reasonably valid to state that it (i.e. λ) is invariant with temperature. Fig. 5b shows Kn and the relative error representing the overestimation of $\bar{J}$ as a result of neglecting Knudsen diffusion. Fig. 5b indicates that Kn needs to be less than 0.1 to have an error less than 10% and this is where d_p should be more than 1.5 µm. Evidently, ignoring Knudsen diffusion for typically-used membranes (where d_p is between 0.1 and 1 µm) results in an unacceptable overestimation of $\bar{J}$ (up to ~ 160 %).

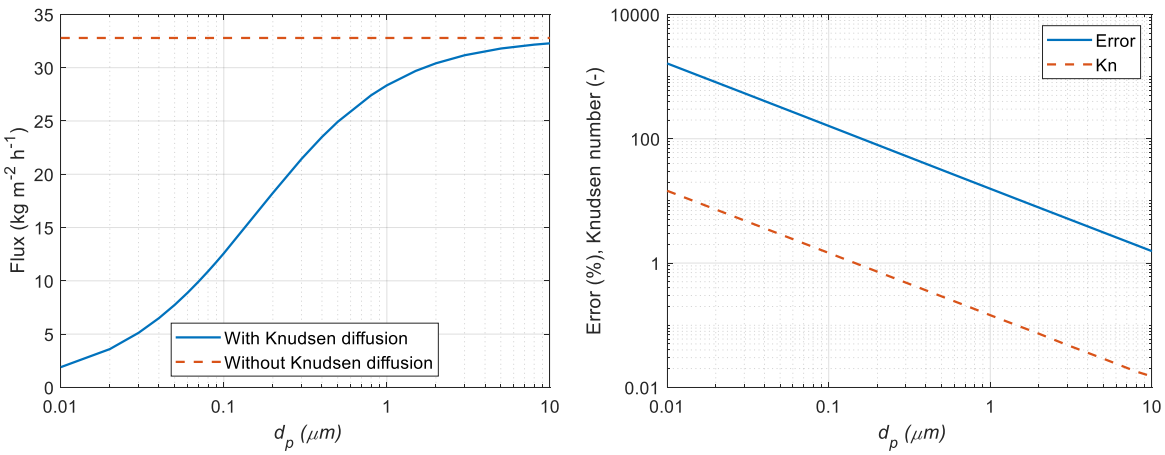

Fig. 5 (a) The transmembrane flux of water vapour ($\bar{J}$) as it changes with the average pore diameter of the membrane (d_p) with/without considering Knudsen diffusion and (b) Knudsen number (Kn) and the relative error (representing the overestimation in $\bar{J}$ as a result of neglecting Knudsen diffusion) as functions of d_p.

3.3 Binary mixture versus ternary mixture

It is rather convenient to assume that the gas mixture within the membrane is binary (water vapour and air) rather than ternary (water vapour, nitrogen and oxygen gases). Namely, a rather simple equation (Fick's law) is normally used for binary mixtures to estimate the flux of water vapour ($\bar{J}$). With ternary mixtures, the molecules of water vapour collide with the molecules of the constituents of air: nitrogen and oxygen gases and in this case Maxwell-Stefan (MS) equations are typically used to solve for the fluxes. The solution of multicomponent diffusion (three components or more) is rather complicated because the diffusion equations governing the mass transport process are coupled [37]. Effective diffusivity method is one of the methods that are often used to solve multicomponent diffusion problems to avoid mathematical complexities [38]. Within COMSOL Multiphysics® platform, one of the effective diffusivity methods is presented under the name "mixture-averaged" diffusion model. The equations describing this method are as follows:

$$J = -\left(\rho_m D_i^{eff} \nabla w_i + \rho_m w_i D_i^{eff} \frac{\nabla M_m}{M_m}\right) \tag{21}$$

where w_i is the mass fraction of the species i and D_i^{eff} is the effective diffusivity of the species i which is obtained using the following reciprocal additivity:

$$D_i^{eff} = \frac{\varepsilon}{\tau}\left[\frac{1}{D_i^{Kn}} + \frac{1}{D_i^{m}}\right]^{-1} \tag{22}$$

where D_i^{Kn} is the Knudsen diffusion coefficient of the species i (which is obtained using Eq. (13)). The "mixture-averaged" diffusion coefficient of the species i (D_i^m) is given as:

$$D_i^m = \frac{1 - w_i}{\sum_{i \neq k} \frac{y_i}{D_{ik}}} \tag{23}$$

where y_i is the mole fraction of the species i and D_{ik} is the multicomponent Maxwell-Stefan diffusivity of the pairs i and k which could be, for convenience, replaced by the binary

diffusivity for the pairs i and k for the low density gas mixture [39]. ρ_m is the density of the gas mixture:

$$\rho_m = \frac{pM_m}{RT} \tag{24}$$

where M_m is the molecular weight of the gas mixture:

$$M_m = \left(\sum_i \frac{w_i}{M_i}\right)^{-1} \tag{25}$$

Fig. 6 shows $\bar{J}$ as it changes with d_p using two models: Fick's law and MS equations. The graph shows that, for the given typical operating conditions, the neglect of frictional forces (accounted for in the MS equations [40]) results in (i) a slight underestimation of $\bar{J}$ (up to 6%) in the region where the mass transport is mainly limited by the Knudsen diffusion (0.01 μm < d_p< 0.1 μm) and (ii) an overestimation of $\bar{J}$ in the region where the molecular diffusion starts to play a more profound role (d_p > 0.1 μm). Within this range (i.e. 0.1 – 10 μm), the overestimation of $\bar{J}$ appears to be somewhat acceptable (up to 7%). It should be noted that the frictional forces are the sum of the forces exerted on the species i by other species; they are proportional to the fraction of other species and the difference between the diffusion velocity of the species i and those of other species [40].

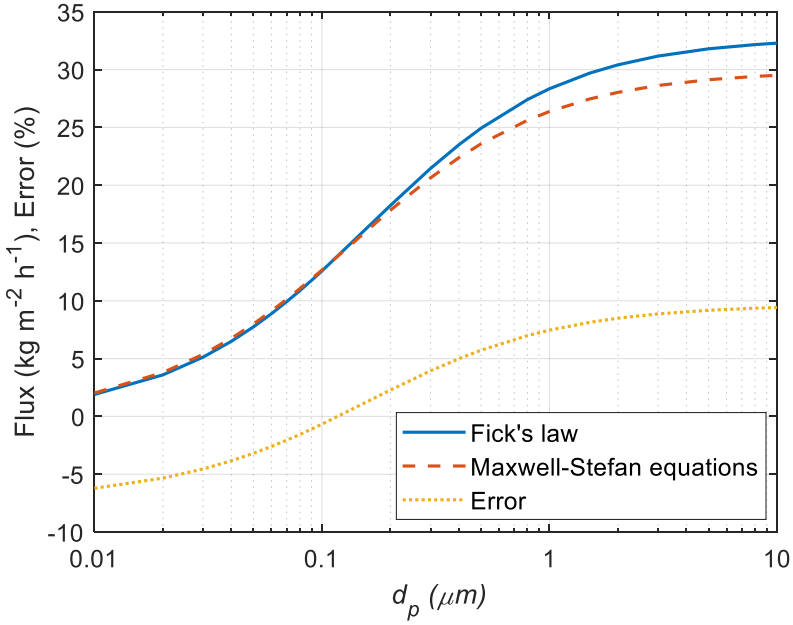

Fig. 6 The transmembrane flux of water vapour ($\bar{J}$) as it changes with the average pore diameter of the membrane (d_p) using Fick's law (solid line) or Maxwell-Stefan equations (dashed line).

3.4 Convection effects

The total pressure within the DCMD module is typically constant and as such there is no pressure difference across the membrane that induces convective mass transport. A high pressure (up to 100 bar [41]) is applied at the side of the membrane that is in contact with the saline solution in the reverse osmosis (RO) process to outweigh osmosis pressure and drive pure water through the membrane. On the other hand, the driving force in the membrane distillation process is the temperature difference across the membrane that induces a difference in the saturation pressure of the solvent (i.e. water vapour in our case). The point of potential interest here is how sensitive the transmembrane flux of water vapour ($\bar{J}$) is to the application of slight pressures (up to say 300 Pa) to the feed channel of the MD module.

The convective flux, induced by the total pressure difference across the membrane, is accounted by the second term in the right side of the following equation (which is an updated version of Eq. (9)):

$$J = \left(-D_{eff}\nabla C_w + \boldsymbol{u}C_w\right)M_w \tag{26}$$

The velocity vector $\boldsymbol{u}$ within the membrane is solved for by Darcy's law:

$$\boldsymbol{u} = \frac{-K}{\mu}\nabla p \tag{27}$$

where K is the permeability coefficient of the membrane (m^2) and μ is the dynamic viscosity of water vapour (~ 1×10^{-5} Pa.s [42]). This permeability coefficient, which is an intrinsic property of the material [43], should not be confused with the permeance (kg m^{-2} h^{-1} Pa^{-1}) or the permeability (the product of the permeance and the membrane thickness) that are often used to express the pressure-driven penetration rates of the separation membranes [44-45]. The permeability for the structures composing of fibres randomly oriented in the lateral direction (resembling the structures of the membranes commonly used in the DCMD modules) is given as follows [46]:

$$K = \frac{\varepsilon}{8\left(\log(\varepsilon)\right)^2}\frac{(\varepsilon - 0.11)^{2.785}}{0.9126(1.785\varepsilon - 0.11)^2}d_f^2 \tag{28}$$

where d_f is, in this work, the average fibre diameter of the membrane. It should be noted that, as the pressure difference is across the membrane, the formula shown in Eq. (28) is for the transverse gas permeability. The permeability coefficients in the lateral directions were, due to their negligible effects, assumed to have the same value as the gas permeability in the transverse direction. The pore diameter of the membrane (d_p) changes as the fiber diameter changes. d_p could be estimated from the Young-Laplace equation [1]:

$$d_p = -\frac{4\gamma\cos\theta}{LEP} \tag{29}$$

where LEP is the liquid entry pressure, γ is the surface tension of water (0.072 N m^{-1} at 25°C [1]) and θ is the contact angle that a water droplet makes with the membrane surface (124° [1]). Guo et al. [1] measured the LEP for some electrospun membranes with different d_f values (Fig. 7a); the dots in Fig. 7a are the experimental data which we curve-fit using a power model:

$$LEP = -0.434 d_f^{-1.528} \quad (30)$$

where the units of LEP and d_f are bar and µm, respectively. The above curve-fitting equation (represented by the solid line in Fig. 7a) was used in Eq. (29) to estimate d_p for a given d_f. Fig. 7b and Fig. 7c respectively present the permeability or K (calculated using Eq. (28)) and the pore diameter or d_p (calculated using Eq. (29)) of the membrane for a given range of d_f. Fig. 7d shows how $\bar{J}$ changes with a slight pressure difference of 300 Pa. The results suggest that such a slight pressure difference has almost no positive impact on $\bar{J}$ for d_p less than 1 µm which encompasses the range of d_p that is featured by most of the DCMD membranes (0.1 – 1 µm); the gain is less than 2%. This is due to the extremely low permeability coefficients of the membranes (~ 10^{-14} - 10^{-15} m^2) with the above d_p range (i.e. 0.1 – 1 µm); consult both Fig. 7b and Fig. 7c. Notably, $\bar{J}$ starts to increase exponentially after 1 µm, resulting in about 25% gain with a d_p of around 10 µm (Fig. 7d).

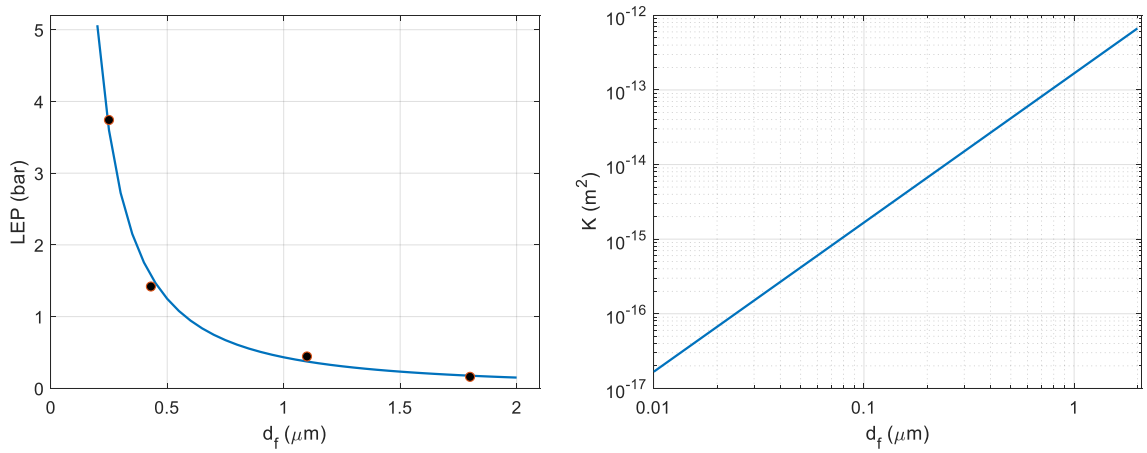

(a) (b)

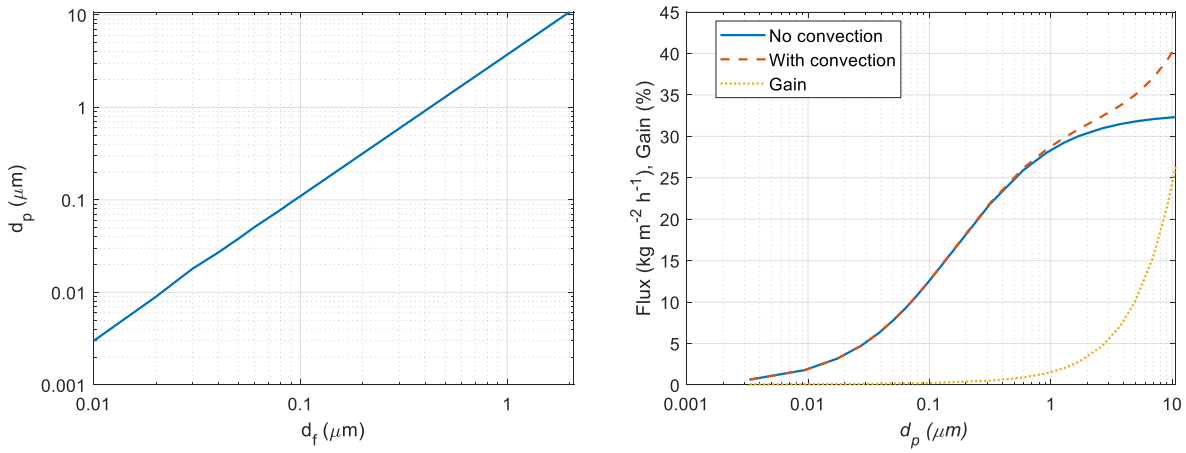

(c) **(d)**

Fig. 7 (a) The liquid entry pressure (LEP) as a function of average fibre diameter of membranes (d_f) (the dots are experimental data [1] and the solid line represents the curve fitting equation of these experimental data), (b) the gas permeability coefficient (K) as a function of the average fibre diameter of the membrane (d_f), (c) the average pore diameter of the membrane (d_p) as a function of the average fibre diameter of the membrane (d_f) and (d) the transmembrane flux of water vapour ($\bar{J}$) as it changes with the average pore diameter of the membrane (d_p) without (solid line) and with (dashed line) a convective flow induced as a result of a slight total pressure difference across the membrane (300 Pa).

3.5 Sensitivity to inlet feed temperature

It was shown in [29] that the inlet feed temperature has the highest impact on the transmembrane flux of water vapour which is one of the operating conditions that could be, compared to the membrane characteristics, easily controlled. It would be therefore of interest to explore the sensitivity of the transmembrane flux of water vapour to all the above assumptions when changing the inlet feed temperature from a typically used one (60 °C) [2, 16, 19] to a lower one (40 °C) or a higher one (80 °C). Table 2 shows that errors/gains arising as a result of the investigated assumptions are in general less with the high inlet feed temperature (80 °C). The regime with this inlet feed temperature is, compared to the other lower inlet feed temperatures, more limited by heat transfer resistance and less sensitive to the mass transport related properties (e.g. diffusion coefficients); this is due to the exponential relationship between the temperature and the saturation pressure of water vapour which is the driving force for the transmembrane flux of water vapour. Notably, the error arising as a result of equimolar assumption very slightly increases (i.e. from 17.3 to 17.4%) when increasing inlet feed temperature from 60 to 80°C. This is mainly attributed to the increased increase of the

molecular diffusion coefficient of water vapour into air, D_{w-a}, at 80°C (0.30%) compared to that at 60°C (0.02%) when switching from equimolar to non-equimolar diffusion. Note that, for a typical membrane pore size range (0.1 – 1 μm), the values of d_p shown in Table 2 are selected based on where the error/gain is a maximum (either 0.1 or 1 μm). Further, the table shows that, with the 80 °C inlet feed temperature, the transmembrane flux is, unlike with the other lower inlet feed temperatures, underestimated (rather than overestimated) if binary diffusion is assumed and Fick's law is subsequently used. This appears to be due to higher increased diffusion coefficient of water vapour when the inlet feed temperature increases from 60 to 80 °C when using Maxwell-Stefan equations rather than Fick's law. Namely, the mixture-averaged diffusion coefficient of water vapour in the ternary mixture (D_w^m) increases by around 9% whereas the diffusion coefficient of water vapour into air in the binary mixture (D_{w-a}) increases by only around 3%.

Table 2 Sensitivity of transmembrane flux of water vapour ($\bar{J}$) to common assumptions with different values of inlet feed temperature (T_{hi}).

Assumption	d_p (μm)	Error/Gain in $\bar{J}$ (%)		
		T_{hi} = 40°C	T_{hi} = 60°C	T_{hi} = 80°C
Equimolar diffusion	1	17.9	17.3	17.4
Knudsen diffusion neglected	0.1	161.7	160.7	150.6
Binary diffusion	1	13.3	7.5	-9.3
Total pressure drop exists (300 Pa)	1	4.0	1.4	0.10

4. Conclusions

A two-dimensional numerical model for a direct contact membrane distillation (DCMD) module, designed for desalination ands wastewater treatment, has been created. The current model is an improved version of a previously developed model presented in [29]; this model considers non-equimolar diffusion rather than equimolar diffusion for the transport of the gas mixture within the membrane. The main motive behind creating the model was to explore the sensitivity of the transmembrane flux of water vapour ($\bar{J}$) to some of the

assumptions/simplification that are commonly used to model the mass transport within the membrane. The below are the key findings of the study:

- For the commonly-used membranes (where the average pore diameter (d_p) is between 0.1 and 1 μm), the error in estimating $\bar{J}$ as a consequence of equimolar (rather than non-equimolar) diffusion assumption could be substantially large (e.g. ~ 17 % with 1 μm d_p) to be overlooked.
- Ignoring Knudsen diffusion for typically used membranes result in an unacceptable overestimation of $\bar{J}$ which could be more than 150%. d_p should be more than 1.5 μm to tolerate the neglect of Knudsen diffusion.
- Fick's law (rather than the more complex and computationally expensive Maxwell-Stefan equations) appears to be safely used to model the transport of water vapour within the commonly-used membranes.
- Slight total pressure differences (≤ 300 Pa) has no positive impact in boosting $\bar{J}$ of the distillation module equipped with the normally-used membranes and this is due the extremely low permeability coefficients of these membranes (~ 10^{-14} - 10^{-15} m^2).
- The error/gain values due to the use of the above-mentioned assumptions become less with relatively high inlet feed temperatures (e.g. 80 °C) as the regime becomes more limited by the heat transfer resistance with such temperatures.

Nomenclature

a	*Activity coefficient*
h_{fg}	*Heat of vaporisation/condensation (J kg^{-1})*
C_p	*Specific heat capacity (J mol^{-1} K^{-1})*
D_{Kn}	*Knudsen diffusion coefficient (m^2 s^{-1})*
D_{w-a}	*Normal (ordinary) diffusion coefficient of water into air (m^2 s^{-1})*
$\bar{J}$	*Average mass transmembrane flux (kg m^{-2} s^{-1})*
d_f	*Average fibre diameter of the membrane (m)*

d_p	*Average pore diameter of the membrane (m)*
p_s	*Saturation pressure (Pa)*
C	*Molar concentration (mol m^{-3})*
K	*Permeability coefficient (m^2)*
Kn	*Knudsen number*
LEP	*Liquid entry pressure (Pa)*
M	*Molecular weight (kg mol^{-1})*
N	*Transmembrane molar flux (mol m^{-2} s^{-1})*
R	*Universal gas constant (J mol^{-1} K^{-1})*
T	*Temperature (K)*
k	*Thermal conductivity (W m^{-1} K^{-1})*
p	*Pressure (Pa)*
q	*Heat flux (W m^{-2})*
w	*Mass fraction*
y	*Mole fraction*
$\boldsymbol{n}$	*Normal vector*
$\boldsymbol{u}$	*Velocity vector (m s^{-1})*
α	*Fitting parameter in Eq. (15)*
β	*Fitting parameter in Eq. (15)*
γ	*Surface tension (N m^{-1})*
ε	*Membrane porosity*
θ	*Contact angle (°)*
λ	*Mean free path (m)*
μ	*Dynamic viscosity (Pa s)*
ρ	*Density (kg m^{-3})*
τ	*Membrane tortuosity*

Subscripts/superscripts

a	*Air*
h	*Hot*

c	*Cold*
eff	*Effective*
g	*Gas*
i	*Inlet; Species i*
k	*Species k*
l	*Left*
m	*Gas mixture*
r	*Right*
s	*Solid*
w	*Water*

Acknowledgments

The authors would like to thank the Institutional Links Newton-Mosharafa Fund (261749278 and STIFA-27653) and Research England QR GCRF Institutional Allocation (X/165302) for their financial support.

Appendix A

The following temperature-dependent polynomials were used to estimate the density (ρ), dynamic viscosity (μ), specific heat capacity at constant pressure (C_p) and thermal conductivity (μ) of the flowing fluid in the feed and permeate channels (i.e. liquid water) [30]:

$$\rho = 838.466 + 1.401T - 3.011 \times 10^{-3}T^2 + 3.718 \times 10^{-7}T^3 \quad \text{(A.1)}$$

$$\mu = 1.38 - 2.122 \times 10^{-2}T + 1.360 \times 10^{-4}T^2 - 4.645 \times 10^{-7}T^3 + 8.904 \times 10^{-10}T^4 - 9.079 \times 10^{-13}T^5 + 3.846 \times 10^{-16}T^5 \quad \text{(A.2)}$$

$$C_p = 12010.1471 - 80.407T + 0.310T^2 - 5.382 \times 10^{-4}T^3 + 3.625 \times 10^{-7}T^4 \quad \text{(A.3)}$$

$$k = -0.869 + 8.949 \times 10^{-3}T - 1.584 \times 10^{-5}T^2 + 7.975 \times 10^{-9}T^3 \quad \text{(A.4)}$$

Appendix B

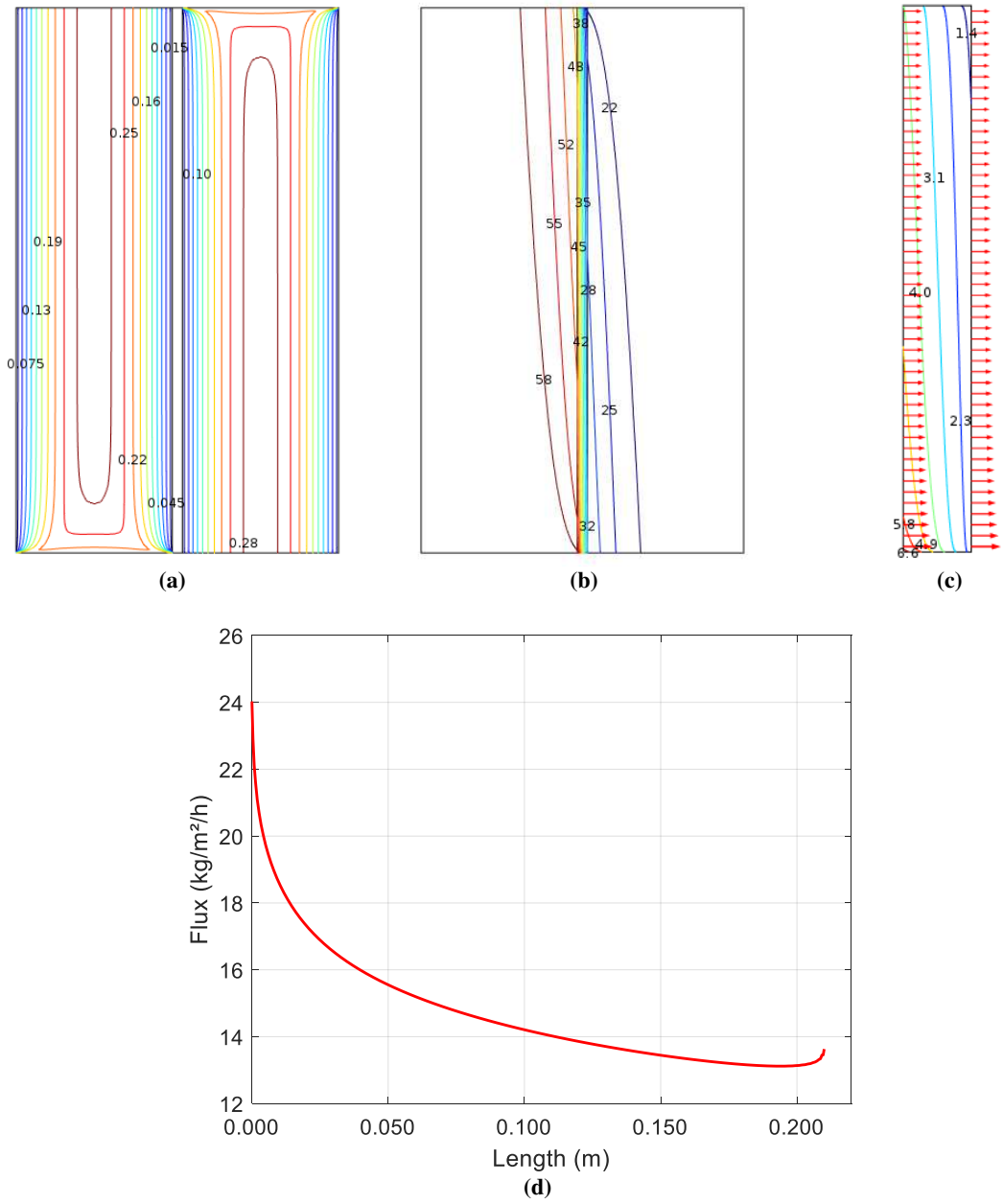

Fig. A1 Contour plots of (a) velocity (m s^{-1}), (b) temperature (°C), (c) concentration of water vapour (mol m^{-3}) in the membrane and (d) flux of water vapour (kg m^{-2} h^{-1}) along the feed-membrane interface. Note that the thickness of the membrane domain in (c) was scaled up 200 times and that the red arrows represent the flux of water vapour (kg m^{-2} h^{-1}) whose magnitudes are shown graph (d). Slightly different profiles were reported in [29] and this is due to considering non-equimolar diffusion for the transport of gas mixture within the membrane in the present work.

468 **References**

[1] F. Guo, A. Servi, A. Liu, K.K. Gleason, G.C. Rutledge, Desalination by Membrane Distillation using Electrospun Polyamide Fiber Membranes with Surface Fluorination by Chemical Vapor Deposition, ACS Appl. Mater. Interfaces 7 (2015) 8225 – 8232.

[2] D.J. Park, E. Norouzi, C. Park, Experimentally-validated computational simulation of direct contact membrane distillation performance, Int. J. Heat and Mass Trans. 129 (2019) 1031 – 1042.

[3] S. Lin, N.Y. Yip, M. Elimelech, Direct contact membrane distillation with heat recovery: Thermodynamic insights from module scale modeling, J. Membr. Sci. 453 (2014) 498 – 515.

[4] J.H. Huang, X.Q. Cheng, Q. Bai, Y.J. Zhang, K. Wang, J. Ma, L. Shao, Ultrafast Poly(sodium methacrylate)-Grafted UiO-66-Incorporated Nanocomposite Membranes Enable Excellent Active Pharmaceutical Ingredient Concentration, Ind. Eng. Chem. Res. 60 (2021) 6287-6297.

[5] J. Zhang, N. Dow, M. Duke, E. Ostarcevic, J.D. Li, S. Gray, Identification of material and physical features of membrane distillation membranes for high performance desalination, J. Membr. Sci. 349 (2010) 295 – 303.

[6] A. Deshmukh, M. Elimelech, Understanding the impact of membrane properties and transport phenomena on the energetic performance of membrane distillation desalination, J. Membr. Sci. 539 (2017) 458 – 474.

[7] K.W. Lawson, D.R. Lloyd, Membrane distillation. II. Direct contact MD, J. Membr. Sci. 120 (1996) 123 – 133.

[8] M.C. García-Payo, M.A. Izquierdo-Gil, C. Fernández-Pineda, Air gap membrane distillation of aqueous alcohol solutions, J. Membr. Sci. 169 (1) (2000) 61–80.

[9] Sarti, C. Gostoli, S. Bandini, Extraction of organic components from aqueous streams by vacuum membrane distillation, J. Membr. Sci. 80 (1993) 21 – 33.

[10] M. Khayet, P. Godino, J. I. Mengual, Theory and experiments on sweeping gas membrane distillation, J. Membr. Sci. 165 (2000) 261-272.

[11] M.M.A. Shirazi, A. Kargari, A Review on Applications of Membrane Distillation (MD) Process for Wastewater Treatment, J. Membr. Sci. Res. 1 (2015) 101-112.

[12] A. El-Abbasi, H. Kiai, A. Hafidi, M.C. Garcia-Payo, M. Khayet, Treatment of olive mill wastewater by membrane distillation using polytetrafluoroethylene membranes, Sep. Purif. Technol. 98 (2012a) 55-61.

[13] D. Qu, D. Sun, H. Wang, Y. Yun, Experimental study of ammonia removal from water by modified direct contact membrane distillation, Desalination 326 (2013) 135- 140.

[14] H. Liu, J. Wang, Treatment of radioactive wastewater using direct contact membrane distillation, J. Hazard. Mat. 261(2013) 307-315.

[15] H.B. Madalosso, R.D.S. Silva, A. Merlini, R. Battista, R.A.F. Machado, C. Marangoni, Modelling and experimental validation of direct contact membrane distillation applied to synthetic dye solutions, J. Chem. Tech. Biotech. 96 (2020) 909-922.

[16] K.W. Lawson, D.R. Lloyd, Membrane distillation, J. Membr. Sci. 124 (1997) 1-25.

[17] L.M. Camacho, L. Dumee, J. Zhang, J. Li, M. Duke, J. Gomez, S. Gray, Advances in Membrane Distillation for Water Desalination and Purification Applications, Water 5 (2013) 94 – 196.

[18] R.J. Silbey, R.A. Alberty, M.G. Bawendi, Physical Chemistry, Chapter 17, 4th edition, 2005.

[19] J. Phattaranawik, R. Jiraratananon, A.G. Fane, Effect of pore size distribution and air flux on mass transport in direct contact membrane distillation, J. Membr. Sci. 215 (2003) 75-85.

[20] T.C. Chen, C.D. Ho, H.M. Yeh, Theoretical modeling and experimental analysis of direct contact membrane distillation, J. Membr. Sci. 330 (2009) 279-287.

[21] I. Janajreh, D. Suwwan, R. Hashaikeh, Assessment of direct contact membrane distillation under different configurations, velocities and membrane properties, App. Energy 185 (2017) 2058-2073.

[22] M. Rezakazemi, CFD simulation of seawater purification using direct contact membrane desalination (DCMD) system, Desalination 443 (2018) 323-332.

[23] M. Ghadiri, S. Fakhri, S. Shirazian, Modeling and CFD Simulation of Water Desalination Using Nanoporous Membrane Contactors, Ind. Eng. Chem. Res. 52 (2013) 3490-3498.

[24] A.M. Alklaibi, N. Lior, Comparative Study of Direct-Contact and Air-Gap Membrane Distillation Processes, Ind. Eng. Chem. Res. 46 (2007) 584-590.

[25] H. Hayer, O. Bakhtiari, T. Mohammadi, Simulation of momentum, heat and mass transfer in direct contact membrane distillation: A computational fluid dynamics approach, J. Ind. Eng. Chem. 21 (2015) 1379 – 1382.

[26] V. Perfilov, A. Ali, V. Fila , A general predictive model for direct contact membrane distillation, Desalination 445 (2018) 181 – 196.

[27] E.A. Mason, A. Malinauskas, Gas Transport in Porous Media: The Dusty-gas Model, (1983)

[28] H. Yu, X. Yang, R. Wang, A. Fane, Analysis of heat and mass transfer by CFD for performance enhancement in direct contact membrane distillation, J. Membr. Sci. 405-406 (2012) 38-47.

[29] M.S. Ismail, A.M. Mohamed, D. Poggio, M. Pourkashanian, Direct contact membrane distillation: a sensitivity analysis and an outlook on membrane effective thermal conductivity, J. Membr. Sci. 624 (2021) 119035.

[30] Material Library. COMSOL Multiphysics® v. 5.2. COMSOL AB, Stockholm, Sweden. 2020.

[31] T.L. Bergman, A.S. Lavine, F.P. Incropera, D.P. Dewitt, Fundamentals of Heat and Mass Transfer, 7th edition, 2011, John Wiley & Sons, US.

[32] A. Alkhudhiri, N. Darwish, N. Hilal, Membrane distillation: A comprehensive review, Desalination 287 (2012) 2-18.

[33] O. Miyawaki, A. Saito, T. Matsuo, K. Nakamura, Activity and Activity Coefficient of Water in Aqueous Solutions and their Relationships with Solution Structure Parameters, Biosci. Biotech. Biochem. 61 (1997) 466-469.

[34] H.J. Hwang, K. He, S. Gray, J. Zhang, I.S. Moon, Direct contact membrane distillation (DCMD): Experimental study on the commercial PTFE membrane and modeling, J. Membr. Sci. 371 (2011) 90-98

[35] A.M. Alklaibi, N. Lior, Membrane-distillation desalination: status and potential, Desalination 171 (2004) 111-131.

[36] S. Roy, R. Raju, Modeling gas flow through microchannels and nanopores, J. App. Phys. 93 (2003) 4870 – 4879.

[37] R. Taylor, R. Krishna, Multicomponent Mass Transfer, Chapter 5, 1st ed., 1993.

[38] R. Taylor, R. Krishna, Multicomponent Mass Transfer, Chapter 6, 1st ed., 1993.

[39] Transport of Concentrated Species Documentation. COMSOL Multiphysics® v. 5.2. COMSOL AB, Stockholm, Sweden. 2021

[40] J.A. Wesselingh, R. Krishna, Mass Transfer in Multicomponent Mixtures, Chapter 4, 1st ed., 2000.

[41] K.P. Lee, T.C. Arnot, D. Mattia, A review of reverse osmosis membrane materials for desalination—Development to date and future potential, J. Membr. Sci. 370 (2011) 1 – 22.

[42] V. Teske, E. Vogel, E. Bich, Viscosity Measurements on water Vapor and Their Evaluation, J. Chem. Eng. Data 50 (2005) 2082-2087.

[43] O.M. Orogbemi, D.B. Ingham, M.S. Ismail, K.J. Hughes, L. Ma, M. Pourkashanian, Through-plane gas permeability of gas diffusion layers and microporous layer: Effects of carbon loading and sintering, Int. J. Hydrogen Energy 91 (2018) 270-278.

[44] J.H. Huang, X.Q. Cheng, Y.D. Wu, Y.Q. Zhang, S.W. Li, C.H. Lau, L. Shao, Critical operation factors and proposed testing protocols of nanofiltration membranes for developing advanced membrane materials, Adv. Comp. Hybrid Mat. in press (https://doi.org/10.1007/s42114-021-00334-w).

[45] J. Guo, H. Bao, Y. Zhang, X. Shen, J.K. Kim, J. Ma, L. Shao, Unravelling intercalation-regulated nanoconfinement for durably ultrafast sieving graphene oxide membranes, J. Membr. Sci. 619 (2021) 118791.

[46] M.M. Tomadakis, T.J. Robertson, Viscous Permeability of Random Fiber Structures: Comparison of Electrical and Diffusional Estimates with Experimental and Analytical Results, J. Comp. Materials 39 (2005) 163-188.